

Problematics of friction in a high-speed rubber-wheel system: A case study of irregularly rough steel in water lubricated contact

A. Ismailov^a, M. Järveläinen^a, E. Levänen^a

^aLaboratory of Materials Science, Tampere University of Technology, P.O.Box 589, FIN-33101 Tampere, Finland

Abstract

A custom-made slurry-type high-speed rubber wheel wear testing system was modified for measuring friction. Friction behaviour of irregularly rough steel against CSM-rubber in water-lubricated contact at a velocity range of 1.7 - 17 m/s was investigated. A noticeable friction maximum was observed near the midpoint of the range extremities, at 6.7 – 8.3 m/s, and the resulting wear marks on steel specimens also suggested the highest severity of contact at these medium speeds. Higher end of sliding velocity range returned friction to lower levels and less wear was observed. This was interpreted as a product of reduction in frictional heat due to slight improvement in mixed lubrication. In conclusion, the peculiar friction behaviour was interpreted as a system-specific anomaly, implying that similar problematics could be encountered in other rubber wheel test systems as well.

Keywords: rubber wheel, sliding friction, wear testing, high-speed, water, steel

1. Introduction

New wear-resistant and friction-related material solutions are commonly tested with standardized procedures, such as the ASTM G99 pin-on-disk[1] or the ASTM G65 rubber wheel sand abrasion test[2]. However, the usefulness of experimental data acquired with standardized tests is very limited, since they only enable reliable comparison of materials within certain boundaries of parameters. In order to reliably test and compare materials' performance potential for a specific application, the test procedure has to be selected and, in some instances, modified to correspond with the process conditions as closely as possible. Rubber wheels are commonly used for wear testing in wide range of parameters, both in dry and lubricated conditions. Incorporating friction measurement into a rubber wheel system is a natural evolution of the test setup when more information on various surface interaction phenomena is required. However, rubber has a very peculiar sliding friction behaviour that needs to be considered both in wear testing and when measuring friction in such systems.

This study reports the friction behaviour observed in a wet high-speed sliding test setup when testing naturally rough hot rolled steel surfaces against smooth rubber. The applied sliding velocities were uniquely high for a rubber wheel wear test system, ranging from 1.7 m/s to nearly 17 m/s. Even though one of the famous Laws of Friction dictates that "friction force is independent of sliding velocity" [3], pioneering experimental and theoretical works on rubber friction by Roth et al.[4], Grosch[5,6], Barquins[7], Roberts[8], Persson et al.[9–12], Heinrich[13], Klüppel[14] and Le Gal[15,16] report in great detail how sliding friction of rubber is affected by changes in sliding velocity and other system parameters, like load, the amount and type of lubrication medium, as well as the chemical composition of the sliding surfaces. These works cover frictional behaviour of elastomers in a wide range of sliding velocities from well under 0.1 m/s to over 40 m/s with vastly differing methodologies, though it can be said, that sliding of elastomers against rigid and rough surfaces remains an incompletely understood field in tribology. Nevertheless, the findings and the general concepts developed in said works are considered applicable in the context of this research and are cautiously utilized for explaining the friction measurement results.

2. Theoretical background

The tribological behaviour of rubber and elastomers in general is not completely understood, despite the high significance, considering the widespread use of sliding-related rubber products, such as windscreen wipers and vehicle tires. Wear and friction phenomena related to rubber always take into account the dual nature of rubber friction[5,12], which comprises of the conventionally important surface adhesion and equally important viscoelastic deformation. Due to its low elastic modulus, rubber deforms notably under moderate pressure, causing high static friction by a mechanism of mechanical interlocking, where rubber completely or partially fills cavities of a surface it is pressed against. On the other hand, sliding motion against macroscopically rough surfaces under some loading conditions causes rubber to undergo viscoelastic deformation loops, where a portion of mechanical energy is converted into heat by the friction of entangled elastomer chains and effectively dissipated into the rubber[11].

Adhesion is another, more direct, source of frictional heat. The relative significance of adhesion in elastomer sliding scenarios depends on the real area of contact between the asperities of both surfaces. This surface area, in turn, is dictated by the roughness characteristics as well as the deformation capacity of said surfaces under a given load. In the case of an elastomer against a hard and rough surface, the low elastic modulus of the elastomer becomes a dominant feature, rendering the elastic properties of the hard surface inconsequential[12]. However, some of the surface area obtained by extensive elastic deformation at standstill is not necessarily retained during fast sliding motion, where the viscoelastic properties may not allow for the rubber to “spring back” and fill profile features of certain size or smaller[11]. Therefore, determining the role and influence of the adhesion component compared to the viscoelastic origin is more complex than merely observing the interaction of roughness, load and surface area.

Due to the system under investigation in this article being a water-lubricated one, basic theory of lubricated sliding needs to be considered as well. Contacts in the sliding interface in lubricated conditions are conventionally divided into three main regions of the Stribeck curve[3]: boundary lubrication, mixed lubrication or elastohydrodynamic lubrication (EHL) region, and hydrodynamic (HD) lubrication. In conventional oil lubricated test procedures (e.g. ASTM D 5707 [17]) and applications, the minimum value of friction coefficient is observed in the transition region between mixed and HD lubrication, at a specific range where the dynamic viscosity of the lubricating medium allows for a thin supporting film to form under given normal load and sliding velocity between moving surfaces.

It is well known, that sliding pairs of most materials under normal atmospheric conditions, lubricated or not, are not atomically clean interactions between materials[18]. In moist and water-containing environments the outermost layer on metallic surfaces tends to be hydroxide (-OH) group that is attached to thin metal oxide, and is additionally almost inevitably covered by other impurities from the surroundings. Thus, the strength of adhesion in water-lubricated sliding is, at least in the region where surface asperities interact, dependent on the amount and type of boundary lubricants and impurities.

3. Experimental procedure

3.1 Modified high-speed sliding wear apparatus

Friction measurements were conducted with a high-speed sliding wear test device built specifically to emulate process conditions containing water and hard particles. The construction and operating principle presented in Figure 1 closely resemble that of the ASTM G65 standard cylinder-on-flat type rubber wheel abrasion test, where a test piece is pressed against a rolling rubber-coated drum with predetermined normal force W that is transmitted into the contact by a lever structure. However, contrary to the mentioned standard test, in our test configuration sliding speed as well as normal load were adjustable and water or water-based abrasive slurry could be used instead of dry silica sand. Due to this being a high-speed slurry-type test device, a cover made of hard translucent plastic was used during the test runs. Formation of wear particles could not be confirmed due to the large size of the water container and the unavoidable presence of residual impurities in the wear-testing device.

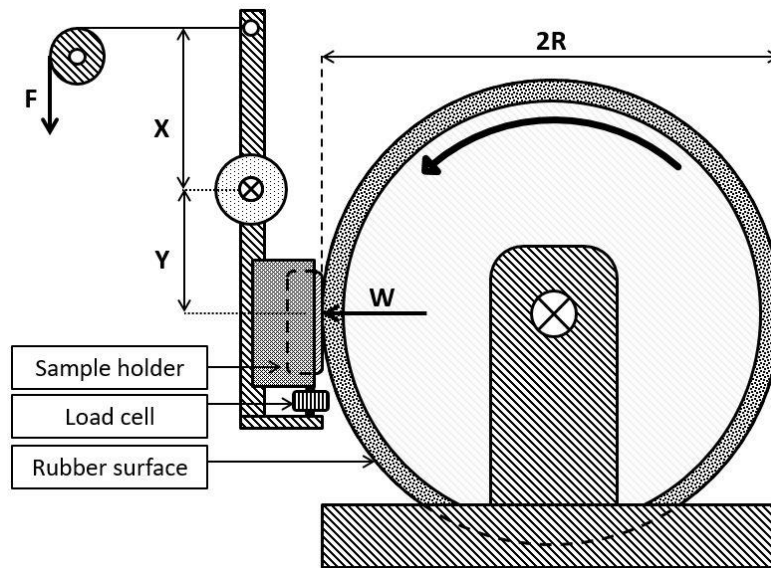


Figure 1 Friction measurement principle (parameter details in Table 1)

The conditions produced by this testing configuration fall under the category of conventional macrotribology, where contact mechanics are severe and typically result in some degree of wear, and are thus representative of those commonly encountered in rubber wear tests and friction studies. Friction was the point of interest in this study, and thus wear was intentionally minimized by using tap water without abrasive particles as a sliding medium. Fifty litres of room temperature tap water was circulated in a closed loop and fed into the contact interface during the test runs.

The tests were carried out in ambient conditions. The sliding velocity range and other relevant test parameters are presented in Table 1. Test duration and normal load were kept constant, 60 min and 46.9 N, respectively. The two adjusted parameters were the sliding velocity v and the associated sliding distance l . Fixed test duration of 60 minutes produced sliding distances that correlated linearly with the sliding velocities.

Table 1: Test run parameters, See Figure 1 for clarification.

High-speed sliding wear/friction test equipment	
Sliding velocity, v [m/s] (m/min)*	1.7(100), 3.3(200), 5.0(300), 6.7(400), 8.3(500), 12.5(750), 16.7(1000)
Test duration, t [min]	60
Sliding distance, l [km]	6.0, 12, 18, 24, 30, 45, 60 (dictated by sliding velocity)
Load, F [N]	37.5
Lever ratio x/y	1.25
Normal load, W [N]	46.9
Medium	Water, feed $\sim 0.26 \text{ m}^3/\text{h}$

* Velocity converted to m/s from m/min of the test equipment control software

Friction force was measured with HBM u9b can-type load cell incorporated into the sample holder. A Datalogger DT80 (Thermo Fisher Scientific Australia Pty Ltd) datalogger was used for data collection and the measurement frequency was set to 1 Hz, which equals 3600 data points for each 60-minute test. A combined error margin of $\pm 3.2\%$ based on relative sensitivity deviation, temperature effects, linearity error and possible creep of the load cell was applied to friction data analysis.

3.2 Rubber contact properties

The rubber coat on the drum was a 11-mm thick layer of chlorosulfonated polyethylene (CSM), which, based on the equipment having been used for wear testing for hundreds of hours before friction instrumentation, was considered permanently unchanged by the friction measurement tests presented in this study. The relative radius of curvature in this cylinder-on block geometry was 265 mm. The relevant properties of rubber wheel contact are listed in the Table 2.

Table 2 Rubber wheel specifications and contact features

Radius of curvature, R [mm]	265
Contact width, L [mm]	16
Rubber coat thickness [mm]	11
Shore A hardness of rubber surface, s^*	67.4 (1s), 63.7 (15s)
Young's modulus of rubber layer, E [MPa]**	4.93 (1s), 4.21 (15s)
Contact length, b [mm]***	~24.0
Maximum contact pressure at standstill, p_{max} [MPa]****	0.15

*Averages of 10 measurements, rubber thickness 10mm

**Determined from Shore A hardness by Eq. (3)

***Determined by Eq. (1)

****Determined by Eq. (2)

The surface hardness of the rubber was determined from a dry room-temperature surface of the wheel with a portable hardness tester (AFFRI, Italy) using Shore A durometer for instantaneous (within 1 second of compression) hardness measurements as described in ASTM D2240 standard[19]. Delayed hardness (15 seconds of compression) is reported for reference only. The hardness results were then used for calculating an approximation value for Young's modulus in accordance with Meththananda et al. [20] with Gent's equation:

$$E = \frac{0.0981(56+7.66s)}{0.137505(254-2.54s)} \quad (1)$$

The measured Shore A hardness values fall slightly outside the range of 30.2-62.9 reported in [20], while still being very close, in our opinion not hindering the utilization of Eq. (1). The maximum contact pressure p_{max} of a cylinder contact was calculated as per [21]:

$$p_{max} = \frac{2W}{\pi bL} \quad (2)$$

where b is contact half-length, which can be derived from the basic relation between normal load W , poisson's ratio ν , Young's modulus E , contact width L and radius of curvature R in a two cylinder contact as follows[21]:

$$b = \sqrt{\frac{4W \left[\frac{1-\nu_1^2}{E_1} + \frac{1-\nu_2^2}{E_2} \right]}{\pi L \left(\frac{R_1+R_2}{R_1R_2} \right)}} \quad (3)$$

where subscript 1 indicates rubber and 2 indicates steel, respectively. To adjust for cylinder-on-block geometry, the term $(R_1+R_2)/R_1R_2$ is reduced to $1/R_1$, since the radius of curvature of the sample surface R_2 approaches infinity. Additionally, since the difference between Youngs moduli in our system is several orders of magnitude, 193 GPa for AISI 316L (see Table 4) and less than 5 MPa for the CSM rubber surface respectively (see Table 2), all of the elasticity can be attributed to rubber with negligible effect on the equation outcome, and $(1-\nu_2^2)/E_2$ can be eliminated. Finally, by assuming no volume change for the rubber under load and thus a Poisson's ratio $\nu_1=0.5$, Eq. (3) can be reduced to:

$$b \approx 1.13 \sqrt{\frac{W \left[\frac{3}{4E_1} \right] R_1}{L}} \quad (4)$$

which, when applying the values from Table 2, yields $b \approx 12.2$ mm and Eq. (2) then gives $p_{max} \approx 153$ kPa.

3.3 Stainless steel test pieces

Fifty-millimetre-long square bar (20 mm x 20 mm) sections of hot rolled AISI 316L (BE Group Oy Ab, Finland) austenitic stainless steel (Tables 3 and 4) were used as counter surface samples. The corrosion resistance of the 316L is tailored for chemical processing environments and marine applications [22], and it is a common grade of steel to use in load-bearing frameworks subjected to corrosive chemicals. The choice of material was based on availability, cost-efficiency and being close to the intended use cases of testing other than perfectly flat or polished sliding surfaces.

Table 3: Composition of AISI 316L according to supplier specifications

C	Mn	Si	P	S	Cr	Mo	Ni	N	Fe
max 0.03	max 2	max 1	max 0.045	max 0.015	16.5-18.5	2-2.5	10-13	max 0.11	Balance

Table 4: Physical and mechanical properties of AISI 316L[22]

Density (g/cm ³)	Elastic Modulus (GPa)	Coefficient of Thermal Expansion (μm/m/°C)	Thermal conductivity at 100°C (W/m*K)	Specific Heat 0-100°C (J/kg*K)	Yield strength (MPa)	Hardness (HV)
8	193	16	16.3	500	205	155

Steel samples were tested in as-received condition, which means that the hot rolled surface topography was not removed by grinding or polishing. The bar sections were washed in ethanol (ETAX Ba) and subsequently dried in a stream of hot air. There were seven samples in total, one for every sliding speed presented in Table 1.

3.4 Surface characterization

The changes in surface characteristics were analyzed by visual inspection, digital photography of contact area and by measuring surface roughness parameters with profilometer. Surface roughness parameters of as-received and tested pieces discussed in section 4.3 were extracted from area measurement data acquired with an optical interferometer (Veeco WYKO NT1100) using the VSI (vertical scanning interferometry) mode with a 1.0x field-of-view lens, as well as 2.5x and 5.0x objectives, resulting in 2.4 mm x 1.9 mm and 1.2 mm x 0.92 mm surface areas, respectively. The measurement data was analysed in WYKO Vision®-software using the built-in tools. A “plane fit”-feature was utilized to eliminate most of the unavoidable tilt from the measured datasets. Relevant surface roughness parameters are stated as “S_x”, three-dimensional equivalents to the standard two-dimensional R_x-values, subscript “x” denoting any of the standard parameters.

4. Results and discussion

4.1 Friction

The seven friction measurement runs are presented in Figure 2 as a function of sliding distance. Only overall trend and static stages in sliding friction behaviour could be examined, due to minute changes being outside the capabilities (accuracy) of the data acquisition equipment. The 1 Hz data acquisition rate did not allow for accurate determination of static friction values in the beginning and the end of the tests when the wheel was accelerated and decelerated. Furthermore, depending on the target velocity, the initial acceleration of the rubber wheel to full speed can take up to a minute, which is why the Figure 2 shows the data starting from 100 seconds into the test, where the sliding velocities had become steady for all the velocities used here. The stated error margin of ±3.2% was based on the load cell specifications, and was applied to all data that contained friction measurements.

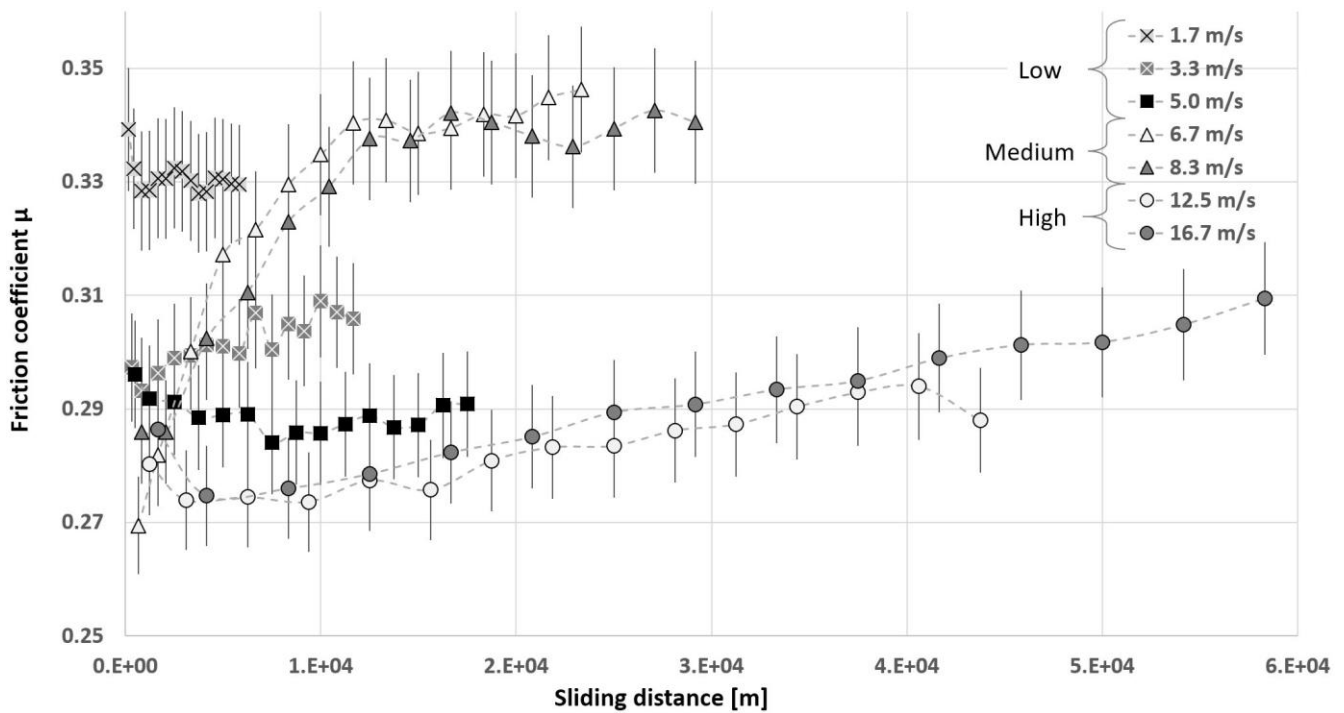


Figure 2 Evolution of friction coefficient over 60-minute tests, where sliding distance is directly determined by sliding velocity

Despite the significant error margin of this experimental friction measurement instrumentation, three types of distinct friction progression were observed: Low speed region (1.7-5.0 m/s) showed that an increase in sliding velocity lowered the friction as could be predicted by looking at studies from Grosch[6] and other subsequent studies, where the lower friction at higher sliding velocities is attributed to increased frictional heat and the resulting softening (decreased Young's modulus). The 6.7m/s and 8.3m/s velocities produced an anomaly, where friction increased radically during the first 30 minutes and stabilized shortly thereafter. In high-speed region (12.5 m/s and 16.7 m/s) a stable increase in friction spanning the entire duration of the test runs was observed and the overall friction behaviour appears again more similar to the low-speed region, giving even lower (initial) friction. The difference between all initial and final values for sliding friction are presented in Figure 3.

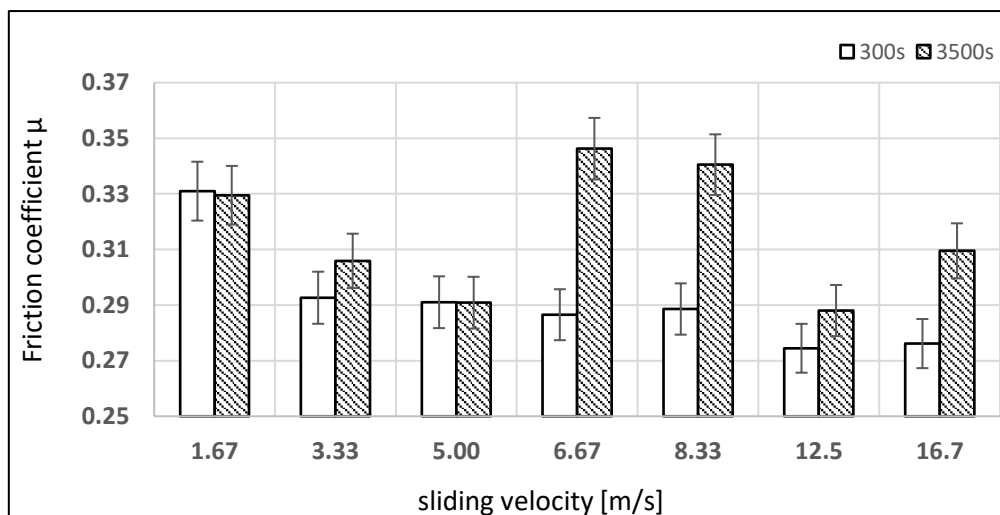


Figure 3 Friction coefficient at the beginning (300s) and the end (3500s) of each test run.

Since the case of steel sliding against rubber in water is very different from ideal lubricated bearings, theory of lubricated sliding must be applied in a very general manner. Forming a complete lubrication layer between smooth rubber and relatively rough counter surface with low-viscosity medium such as water would additionally require very fast relative motion[23]. Indeed, based on the overall magnitude of the measured friction coefficients (0.27 - 0.35), despite being an order of magnitude lower than what had been measured in some non-lubricated and relatively non-

contaminated contacts[4,5,7], it is evident that the contact is not close to complete hydrodynamic lubrication at any of the measured velocities. However, initial friction forces at 300 seconds for all measurements fit the general assumption that increasing sliding velocity, even in water-lubricated sliding, decreases friction due to increased frictional heat by slight improvement in lubrication, given a broad enough contact geometry[6]. Towards the end of the test runs, at 3500 seconds, the friction was significantly higher for the medium range (6.7 m/s and 8.3 m/s), and mildly increased for the highest velocity (16.7 m/s). The results for 3.33 m/s and 12.5 m/s are not definitive due to the margin of error, though based on Figure 2, the latter follows the more unambiguous trend of 16.7 m/s rather closely and is thus interpreted as a part of the same general pattern.

4.2 Surface evolution of steel

Varying levels of surface evolution were evident after 60 minutes of testing for original steel surfaces. The fact that measurements were run in water without abrasive particles means, that the origin of surface evolution can only be attributed to frictional heating occurring in the boundary lubrication conditions as reported by Roberts[8] and many studies thereafter. Key features of steel surface evolution for this friction-oriented study are presented in Figure 4. Digital photographs of tested surfaces were cropped and converted into high-contrast black and white images for maximum clarity.

The sliding velocity of 1.7 m/s produced a clear wear mark on the hot rolled steel surface. This is well in line with the high coefficient of friction that was observed for the lowest velocity and it works as a reference point for the other measurements. In 8.3 m/s the wear mark is even more pronounced, and instead of hourglass shape the altered area is rather square, which indicates more uniformly severe conditions throughout the contact. At the highest value of $v = 16.7$ m/s, the hourglass shape of the contact is even more pronounced than in 1.7 m/s and the centre region is clearly less affected. Even though we assume that lubrication regime does not change within the sliding velocity range tested here, it is still possible to attribute the lower frictional stresses and consequently lower severity (contact temperature) to slightly improved boundary lubrication at higher sliding velocity[8].

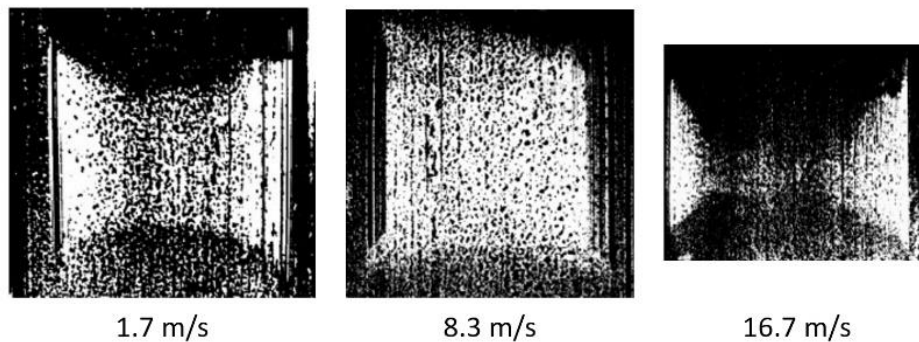


Figure 4 Surface wear marks in crucial velocity ranges. The worn surface portions can be distinguished as light areas against the less reflective, darker background.

The hourglass shape of the wear tracks was caused by the cylinder-on-block contact geometry with the presence of water. Due to higher hydrodynamic fluid pressure, the centre of the contact moved towards mixed lubrication in lower sliding velocities than the edges. The edges of the contact area on the steel surface were under lower fluid pressure due to water being able to escape the interface, and were thus more readily exposed to more severe (higher contact pressure) boundary lubricated contact with the wheel, resulting in higher frictional heat that ultimately causes increased wear. Similar distribution of contact and fluid pressures had been mathematically predicted for soft water-lubricated journal bearings under mixed lubrication conditions[24], and had also been considered when analyzing wear of bushings in that context [25].

The value of maximum contact pressure during motion may vary greatly due to differences in contact characteristics evident from wear tracks shown in Figure 4. Momentary local pressure maxima during sliding are likely much higher than $p_{max} \approx 153$ kPa calculated earlier, due to the real area of contact being smaller than apparent area of contact.

4.3 Surface roughness in relation to friction

Roughness analysis focused on the center region, where the interaction between rubber and steel varied the most due to assumed fluid pressure maximum and the effects it may have on lubrication. Measurement points on an unrelated, severely worn sample are presented in Figure 5.



Figure 5: A typical wear track on an unrelated AISI 316L sample. Water feed and sliding direction is stated with an arrow and roughness measurement spots indicated by circles, pertaining to the numbering used in Table 5.

There were two distinct levels of roughness on a hot rolled 316L surface, as is apparent from profile scans presented in Figure 6: the roughness of the levelled surface and macro-scale open porosity that adds discontinuity to the contact interface. The fine roughness of the levelled surface is more affected by wear than the large open pores, which can be found on both as-received and worn samples. These different length scales of surface texture contribute differently to rubber friction[12]. Short-range shallow roughness on levelled sections can be filled by deformed rubber, contributing mostly to adhesion during sliding. The long-range roughness consisting of larger pits, most likely is not completely filled under the relatively low loads used here, regardless of sliding velocity. However, water-lubricated contacts for rubber against a rough surface may produce so called “the sealing effect”[26], where the effective overall roughness of the surface becomes lower due to water being trapped in pits that form the long-scale roughness. This further amplifies the role of adhesion. By this reasoning we draw a conclusion, that the steady increase of friction at 6.7 m/s and 8.3 m/s during the first ~30 minutes (see Figure 2) is due to the the short-range roughness being removed by wear, enabling a more complete contact and consequently, better adhesion over the smooth surface. The steady friction phase following the initial rise would then represent the point where this smoothing is complete, and only the long-range roughness remains. Similarly, the slow rise in friction at high velocity range would be the result of wear, but inhibited by slightly improved lubrication.

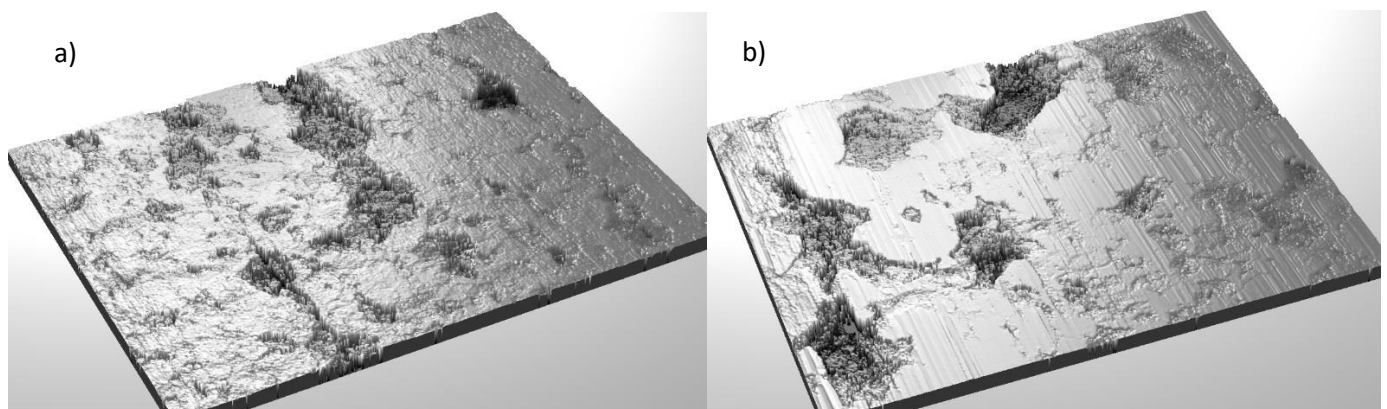


Figure 6: As-received a), and worn b) steel surfaces

When it comes to actual roughness parameters extracted from the surface profiling, the average roughness S_a is a poor descriptor of surface topography if presented without context. Ten-point mean roughness S_z describes maximum height of the roughness profile calculated from top five peaks and the five lowest valleys, and is far more useful for

measuring wear. The skewness parameter S_{sk} depicts the asymmetry of the profile in relation to the mean plane, negative values indicating a predominance of valleys. The complete roughness data is shown in Table 5.

Table 5: Roughness measurement data for steel surfaces presented in μm . (₁before, ₂after, *an average of all 7 samples before testing)

v [m/s]	S_{a1}	S_{a2}	ΔS_a	S_{z1}	S_{z2}	ΔS_z	S_{sk1}^*
1.7	2.0	1.5	-0.5	21.2	22.6	1.4	
3.3	2.0	1.5	-0.5	21.1	19.3	-1.8	
5.0	1.9	1.0	-0.9	21.6	13.7	-7.9	
6.7	2.3	3.5	1.2	25.1	27.1	2.0	-3.1
8.3	1.3	1.5	0.2	19.2	21.6	2.4	
12.5	1.9	1.6	-0.3	22.9	19.3	-3.6	
16.7	1.5	1.5	-0.0	16.6	15.7	-0.9	

Figure 7 presents the changes in ten point average roughness projected on final sliding friction values. It would be expected, that wear-related smoothing discussed earlier and presented in Figure 4 and Figure 6 would cause S_z to decrease as the deep pits become shallower. However, as is apparent by examining Table 5 and Figure 7, the heterogeneity of the hot rolled surfaces makes numerical comparisons of roughness parameters nearly trivial. The ten-point roughness measurement results show a rather erroneous increase in roughness for samples that were shown to have observable wear displayed in Figure 4.

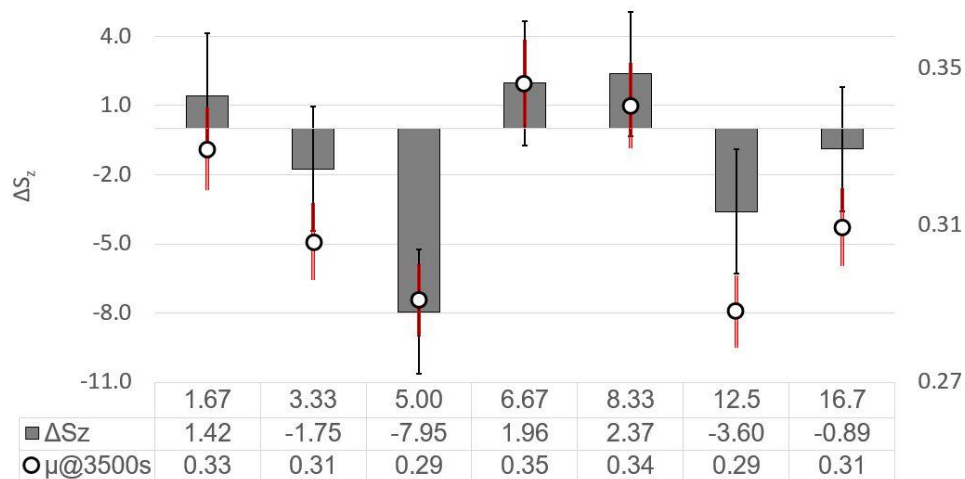


Figure 7: The relative change in ten-point roughness S_z compared to final friction values at 3500 seconds for each velocity.

5. Conclusions

Friction force evolution of hot-rolled, naturally rough AISI 316L stainless steel blocks against CSM-rubber coated wheel in water-containing conditions suggested there being an increase in severity of contact in the 6.7-8.3 m/s region. This region of increased frictional stress was interpreted as a system-specific feature, mostly arising from the friction behaviour of the rubber. The evolution of friction in every separate test run was attributed to the observable wear of the steel specimens. While these variations in friction coefficient did not point to a shift in lubrication regime, the role of slightly improved lubrication cannot be dismissed as a major contributor to lower friction in the highest sliding velocity at 16.7 m/s. This conclusion was supported by the appearance of the wear mark on said sample, where the assumed fluid pressure maximum at the centre of the wear track resulted in very low wear.

We recommend exercising caution when interpreting the results of both wear- and friction testing conducted on rubber wheel systems, especially in high-velocity sliding against rough surfaces. The range of parameters where frictional anomalies may occur should be identified for all unique rubber wheel systems, to avoid misinterpreting the wear test results. Slurry-based test rigs, while certainly providing overall lower friction and wear rates compared to their dry counterparts, may still have noticeable variation in friction and severity of contact within the variable test parameters. Ours was one such case.

Acknowledgements

The work has been done within FIMECC Ltd and its DEMAPP program. We gratefully acknowledge the financial support from Tekes and Valmet Technologies Ltd.

References

- [1] ASTM International, ASTM G99-17, Standard Test Method for Wear Testing with a Pin-on-Disk Apparatus, West Conshohocken, PA, 2017. doi:10.1520/G0099-17.
- [2] ASTM International, ASTM G 65-4 , 2004, "Standard Test Method for Measuring Abrasion Using the Dry Sand / Rubber Wheel," West Conshohocken, PA, 2016. doi:10.1520/G0065-16.
- [3] I.M. Hutchings, Tribology: Friction and wear of engineering materials, 4th ed., Arnold, London, 1992.
- [4] F.L. Roth, R.L. Driscoll, W.L. Holt, Frictional Properties of Rubber, *Rubber Chem. Technol.* 16 (1943) 155–177. doi:10.5254/1.3540095.
- [5] K.A. Grosch, The Relation between the Friction and Viscoelastic Properties of Rubber, *Rubber Chem. Technol.* 37 (1964) 386–403. doi:10.5254/1.3540331.
- [6] A. Grosch, THE SPEED AND TEMPERATURE DEPENDENCE OF RUBBER FRICTION AND ITS BEARING ON THE SKID RESISTANCE OF TIRES, *Phys. Tire Tract.* (1974) 143–165.
- [7] M. Barquins, A.D. Roberts, Rubber friction variation with rate and temperature: Some new observations, *J. Phys. D. Appl. Phys.* 19 (1986) 547–563. doi:10.1088/0022-3727/19/4/010.
- [8] A.D. Roberts, Temperature rise when rubber slides, *J. Nat. Rubb. Res.* 2 (1987) 255. https://scholar.google.com/scholar?hl=en&q=A.D.+Roberts%2C+J.+Nat.+Rubb.+Res.+%281987%29+255+&btnG=&as_sdt=1%2C21&as_sdtp=
- [9] B.N.J. Persson, Sliding friction, *Surf. Sci. Rep.* 33 (1999) 83–119. doi:10.1016/S0167-5729(98)00009-0.
- [10] B.N.J. Persson, Theory of rubber friction and contact mechanics, *J. Chem. Phys.* 115 (2001) 3840. doi:10.1063/1.1388626.
- [11] B.N.J. Persson, E. Tosatti, Qualitative theory of rubber friction and wear, *J. Chem. Phys.* 112 (2000) 2021. doi:10.1063/1.480762.
- [12] B.N.J. Persson, On the theory of rubber friction, *Surf. Sci.* 401 (1998) 445–454. doi:http://dx.doi.org/10.1016/S0039-6028(98)00051-X.
- [13] G. Heinrich, Hysteresis Friction of Sliding Rubbers on Rough and Fractal Surfaces, *Rubber Chem. Technol.* 70 (1997) 1–14. doi:10.5254/1.3538415.
- [14] M. Klüppel, G. Heinrich, Rubber Friction on Self-Affine Road Tracks, *Rubber Chem. Technol.* 73 (2000) 578–606. doi:10.5254/1.3547607.
- [15] A. Le Gal, X. Yang, M. Klüppel, A. Le Gal, Evaluation of sliding friction and contact mechanics of elastomers based on dynamic-mechanical analysis., *J. Chem. Phys.* 123 (2005) 14704. doi:10.1063/1.1943410.
- [16] A. Le Gal, L. Guy, G. Orange, Y. Bomal, M. Klüppel, Modelling of sliding friction for carbon black and silica filled elastomers on road tracks, *Wear.* 264 (2008) 606–615. doi:10.1016/j.wear.2007.05.002.
- [17] ASTM International, ASTM D5707-11 Standard Test Method for Measuring Friction and Wear Properties of Lubricating Grease Using a High-Frequency, Linear-Oscillation (SRV) Test Machine, West Conshohocken, PA, 2016. doi:10.1520/D5707-16.
- [18] D.H. Buckley, ed., Tribology Series: Surface Effects in Adhesion, Friction, Wear, and Lubrication, in: Elsevier B.V., 1981: pp. 315–428.
- [19] ASTM International, ASTM D2240-15, Standard Test Method for Rubber Property—Durometer Hardness, West Conshohocken, PA, 2015. doi:10.1520/D2240-15.
- [20] I.M. Meththananda, S. Parker, M.P. Patel, M. Braden, The relationship between Shore hardness of elastomeric dental materials and Young's modulus, *Dent. Mater.* 25 (2009) 956–959. doi:10.1016/j.dental.2009.02.001.
- [21] T.A. Stolarski, Elements of contact mechanics, *Tribol. Mach. Des.* (1990) 64–96. doi:10.1016/B978-0-434-91826-3.50006-7.
- [22] MatWeb, Material property data, (2017). <http://www.matweb.com/search/DataSheet.aspx?MatGUID=a2d0107bf958442e9f8db6dc9933fe31&ckck=1> (accessed December 13, 2017).
- [23] Z. liang Xie, N. Ta, Z. shi Rao, The lubrication performance of water lubricated bearing with consideration of wall slip and inertial force, *J. Hydrodyn.* 29 (2017) 52–60. doi:10.1016/S1001-6058(16)60716-3.
- [24] A. de Kraker, R.A.J. van Ostayen, D.J. Rixen, Calculation of Stribeck curves for (water) lubricated journal bearings, *Tribol. Int.* 40 (2007) 459–469. doi:10.1016/j.triboint.2006.04.012.
- [25] W. Litwin, Influence of local bush wear on water lubricated sliding bearing load carrying capacity, *Tribol. Int.* 103 (2016) 352–358. doi:10.1016/j.triboint.2016.06.044.
- [26] B.N.J. Persson, U. Tartaglino, O. Albohr, E. Tosatti, Sealing is at the origin of rubber slipping on wet roads, *Nat. Mater.* 3 (2004) 882–885. doi:10.1038/nmat1255.